Drying of a Fully Saturated Porous Medium With Excess Water Layers: A Numerical Study

Munevver Elif Asar[1]
Department of Mechanical and Materials Engineering,
Center for Advanced Research in Drying
Worcester Polytechnic Institute,
100 Institute Road,
Worcester, MA 01609
e-mail: masar@wpi.edu

Jamal Yagoobi
Department of Mechanical and Materials Engineering,
Center for Advanced Research in Drying,
Worcester Polytechnic Institute,
100 Institute Road,
Worcester, MA 01609

Drying of moist porous media can be very energy inefficient. For example, in the pulp and paper industry, paper drying consumes more than two-thirds of the total energy used in paper machines. Novel drying technologies can decrease the energy used for drying and lessen the manufacturing processes' carbon footprint. Developing next-generation drying technologies to dry moist porous media may require an understanding of removing moisture from a fully saturated porous material with excess water. This paper provides a fundamental understanding of heat and mass transfer in a fully saturated porous medium with excess water. This is relevant, for example, in drying tissue as well as pulp or paper for the purpose of thermal insulation where pressing is preferred to be avoided to overcome the reduction in the sheet thickness. For this purpose, a theoretical drying model is developed where the porous medium corresponds to paper and is assumed to be sandwiched between two excess-water layers (bottom and top). The conjugate model consists of energy and mass conservation equations for each layer. The model is validated with corresponding experimental data. In the model, the thickness of each water layer is calculated as a function of drying time based on local temperature and total moisture content. The numerical model is transient and one-dimensional in space (i.e., in the thickness direction). This paper demonstrates the governing equations, boundary conditions, and results when the saturated porous medium with water layers is heated from one side. Moisture and temperature profiles are estimated in the thickness direction of the porous medium as it dries. [DOI: 10.1115/1.4056068]

Introduction

Drying of moist porous media can be very energy inefficient and can require massive loads of energy. Drying processes can generate substantial greenhouse gas emissions, which significantly impact climate change. For example, almost a quarter (21 TJ/day) of the industrial energy used in the United States is for paper manufacturing, where paper dying is a major step [1]. About 70% of the energy used in papermaking (i.e., paper machine) is consumed during the paper-drying process. Thus, porous media drying, specifically paper drying, is a relevant and crucial topic.

This work uses paper drying as an example of porous media drying. Moist paper is conventionally dried with multicylinder dryers during the paper manufacturing process, and around 90% of paper tons are dried by multicylinder dryers [2,3]. The porous medium can be fully saturated and can contain excess water outside the saturated medium layer. For example, in a paper machine, paper is fully saturated and has excess moisture before the pressing section. In addition, paper-sheet surfaces become fully saturated during the coating section, and excess moisture can be present near these surfaces.

To assess various drying technologies, designers can rely on numerical drying models of porous media. Developing next-generation drying technologies, which includes novel drying methods (e.g., ultrasound-assisted drying [4,5] and electrohydrodynamic drying [6]) to dry moist porous media may require an understanding of removing moisture from a fully saturated porous material with excess water. Recent studies [7,8] have shown that ultrasound-assisted drying mechanisms perform better when the porous medium has a higher initial moisture content. Patel et al. [7] used multiple ultrasonic transducers to dry moist fabric. They concluded that ultrasound had a more significant effect on drying performance when the initial moisture content of the fabric was higher. More recently, Asar et al. [8] have reported drying rates of paper with two initial conditions: (1) unsaturated paper and (2) saturated paper with excess water. The latter case showed a much higher drying rate when the moist samples were placed on an ultrasound-emitting transducer. In addition, Yang and Yagoobi [9] studied experimental electrohydrodynamic drying or drying of moist paper in the presence of an electrically driven vapor extraction force. They demonstrated that the effectiveness of electrohydrodynamic drying is more significant with the higher initial moisture content of the moist paper. In brief, assessing the performance of novel drying technologies may require a drying model for a saturated porous medium with excess water.

Several researchers studied heat and mass transfer in unsaturated (saturation, $s < 1$) porous media such as paper drying. Nissan and Hansen [10] were among the first to model paper drying for a multicylinder paper-drying machine. Seyed-Yagoobi et al. [11] utilized a theoretical model for free-water removal from paper in the drying section of a paper machine. That model estimated the liquid water fluxes by convection and water vapor fluxes by diffusion. They solved for energy and continuity equations that are transient and one-dimensional (1D) in space (in the thickness direction). Further, Asensio and Seyed-Yagoobi [12] presented an improved version of the model, which included an empirical contact-conductance correlation for paper in contact with the dryer surface and the changes in thickness and porosity of paper during drying. Later, Seyed-Yagoobi et al. [13] verified the model by pilot machine trials, in which a gas-fired infrared emitter was combined with multiple-dryer drums for various grades of paper. Moreover, Hoshi et al. [14] established a paper-drying model for paper between a hot dryer roll and a canvas. This study was 1D, transient, and treated liquid water movement by capillary forces and vapor movement by diffusion and advection. Lu and Shen's model [15] similarly modeled the paper-

[1]Corresponding author.

Contributed by the Heat Transfer Division of ASME for publication in the Journal of Heat Transfer. Manuscript received July 16, 2022; final manuscript received October 16, 2022; published online November 22, 2022. Assoc. Editor: Yan Su.

drying process and was verified by data collected from an industrial paper machine. In addition, Sadeghi and Douglas [16] demonstrated a validated model called a McGill paper-drying simulator for multiple heating modes and paper grades. Sadeghi [17] provided an overview of paper drying models. Recently, Anjomshoaa and Salmanzadeh [18] developed a drying model for a paper machine based on empirical relationships without using discretization methods. They have done a sensitivity analysis of the input parameters similar to Kong et al. [19] and Zvolinschi et al. [20]. In addition, a numerical tool was developed by Martin et al. [21] for rapid prediction of industrial paper drying where hot air impinges on the surface of the moving paper sheet. They validated the model using an industrial line with several furnaces for resin impregnated paper. Typically, most drying models use the volume-averaging method explained by Whitaker [22]. Few studies [12,13,23–25] have included the effect of paper's porosity and thickness changes during drying. A recent study by Yan et al. [26] investigated paper drying rate based on Lattice Boltzmann method and reported that porosity has a strong impact on the drying rate during the constant drying state. More information on mass and heat transport models to analyze the drying process in porous media can be found in Vu and Tsotsas [27].

Overall, the models mentioned above use unsaturated papers at the onset of drying and are not applicable for excess water cases. In addition, Carbonell et al. [28] explored postaccidental analysis of a nuclear reactor. They studied dry-outs after boiling bottom-heated saturated porous media (bronze and sand particles) with an overlying plain water layer. However, this study included the boiling phenomenon and is not applicable to relatively low-temperature drying applications such as paper drying.

There is a need to fundamentally understand heat and mass transfer in drying moist porous media, such as paper, with excess water. For example, in paper making, the paper web is pressed after the formation section to remove most of the free water. Pressing happens before the paper web enters the drying section. With novel technologies being developed, such as ultrasound technology, it may be advantageous to remove the excess water during and/or right after the formation section as well as immediately after the pressing section, before the paper web enters the dryer section. Furthermore, it might be preferred to avoid the pressing section to allow for a bulkier paper that can be suitable for insulation purposes. Thus, there is a need for a fundamental understanding of drying saturated paper with excess water. To the authors' best knowledge, drying of a fully saturated porous medium (i.e., paper) with excess water layers has not been previously fundamentally explored. The proposed theoretical model, validated against the experimental data, provides an in-depth detailed analysis.

Theoretical Model

A theoretical model is developed for free water removal during drying a fully saturated porous medium (i.e., paper) with excess water heated by a hot plate from below. This study assumes that the saturated porous medium is sandwiched between two excess-water layers (bottom and top). The surface evaporation from the top is through natural convection. The following sections discuss how to determine the excess water thickness, assumptions, stages of drying, governing equations, boundary conditions and model validation.

Determination of Excess Water Thickness. Saturation (s) is defined as the ratio of liquid volume over the pore volume of a porous medium. A fully saturated porous medium contains the maximum allowable liquid content inside its pores. In other words, all the pores are filled with liquid, and saturation is at its maximum ($s=1$). If the total water content level surpasses this maximum liquid content level, there must be excess water layer(s) outside the fully saturated porous media. The thickness of the excess water layers can be calculated based on the porous medium's moisture content, temperature, and porosity. The calculation of total water layer thickness can be described as follows.

A moist porous sheet comprises three components: fiber, liquid, and air, which are mixed inside the sheet. If these components were unmixed and to be treated as distinct layers, each component would have a thickness (th), as shown in Fig. 1. These thicknesses could be calculated by dividing their mass per unit area by their density. For example, the total thickness of liquid water (th_w) can be shown as Eq. (1). Note that the mass of water per unit area is equivalent to the dry basis moisture content (DBMC) times basis weight (BW)

$$\mathrm{th}_w = \frac{M/A}{\rho_w} = \frac{\mathrm{DBMC}\cdot \mathrm{BW}}{\rho_w} \tag{1}$$

To calculate the total "excess" water thickness ($\mathrm{th}_{w,e}$), the maximum thickness of water that could be contained in the porous media (when $s=1$) is subtracted from the total water thickness. Therefore, by using Eq. (1), the total excess water layer thickness is

$$\mathrm{th}_{w,e} = \frac{(\mathrm{DBMC} - \mathrm{DBMC}_{\mathrm{pm},\,s=1})\,\mathrm{BW}}{\rho_w} \tag{2}$$

Dry basis moisture content of a fully saturated porous media ($\mathrm{DBMC}_{\mathrm{pm},\,s=1}$) is dependent on sheet temperature because the water density (ρ_w) varies with temperature. Note that thermal expansion of fiber is assumed negligible compared to that of water. Increasing sheet temperature decreases the density of water, and for a given pore volume, the water mass contained in this volume would drop. This situation decreases the maximum allowable water mass ($s=1$) that can be contained in the porous media, and DBMC should decline as a result. This study uses the shrinkage model of Asensio and Seyed-Yagoobi [12], and porosity at any given time during drying can be shown in Eq. (3). This porosity equation is combined with the DBMC equation given in Eq. (4) and can be solved for the DBMC value when $s=1$. The resulting $\mathrm{DBMC}_{\mathrm{pm},\,s=1}$ is given by Eq. (5) and ensures a fully saturated porous medium at any sheet temperature during drying

$$\varepsilon = 1 - \frac{1-\varepsilon_{\mathrm{fin}}}{1+\left(\frac{\mathrm{DBMC}\,\mathrm{BW}}{\rho_w \mathrm{th}_{\mathrm{fin}}}\right)} \tag{3}$$

$$\mathrm{DBMC} = \frac{M}{\mathrm{BW}/\mathrm{th}_{\mathrm{fin}}} = \frac{\varepsilon s \rho_w}{\mathrm{BW}/\mathrm{th}_{\mathrm{fin}}} \tag{4}$$

$$\mathrm{DBMC}_{\mathrm{pm},s=1} = \frac{\sqrt{\varepsilon_{\mathrm{fin}}}\,\rho_w \mathrm{th}_{\mathrm{fin}}}{\mathrm{BW}} \tag{5}$$

Assumptions. A few assumptions are made in the theoretical analysis of drying of fully saturated porous medium with excess water, and can be listed as follows. (1) Heat and mass transport within all layers are 1D in the thickness direction (z-dir). In other words, two-dimensional (2D) effects are not accounted for in the model. Hence, evaporation and heat gain or loss from side surfaces are ignored. This is a common assumption for paper drying.

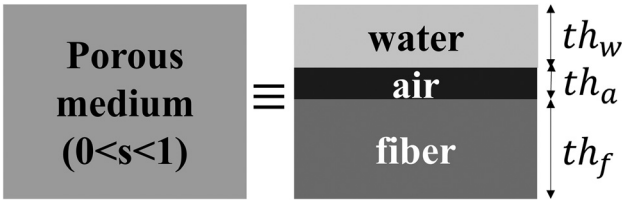

Fig. 1 The components of a moist porous medium and their thicknesses

(2) The effect of gravitational acceleration is ignored. Therefore, there is only heat conduction in the water layers with no Rayleigh-Bénard convection. In fact, Rayleigh number (Ra) (based on maximum temperature difference within water layers and maximum water layer thicknesses) is $\ll 100$ due to the small water layer thicknesses. For small Ra ($Ra < 10^3$), the heat transfer is primarily by conduction across the fluid and buoyancy-driven flow can be ignored [29]. (3) The excess water is equally distributed between the top and bottom of fully saturated paper just before the drying process begins.

Stages of Drying. The drying of a fully saturated porous medium with excess water layers is divided into three stages because each stage has different conditions. A schematic illustrating these drying stages is shown in Fig. 2. Since each layer (control volume) is solved separately, each layer has its own coordinate (z_{bw}, $z_{tw,}$ and z_{pm}), and a "hot plate" heats the water layers and porous medium from below, as shown in Fig. 2. Stage 1 is the first stage of drying, and during this stage, the porous medium is sandwiched between the two excess water layers; therefore, the porous medium remains fully saturated. During stage 1, the top water layer evaporates. When the top water layer is dried, stage 1 ceases, and stage 2 begins. During stage 2, water inside the porous medium is free to evaporate from its top surface, and the bottom water layer feeds the porous media from the bottom. During this stage, the thickness of the bottom water layer diminishes. Stage 3 starts when the bottom layer is dried, and the porous medium directly contacts the hot plate.

The total excess water thickness is calculated by Eq. (2) using the initial DBMC of the porous medium with excess water. It is divided by two to obtain the equally allocated top and bottom excess water layers. At each time-step of the numerical solution of the drying process, the excess water thicknesses are updated, in addition to each layer's temperature profile and moisture content profile in the porous medium. The governing equations are described in the following section.

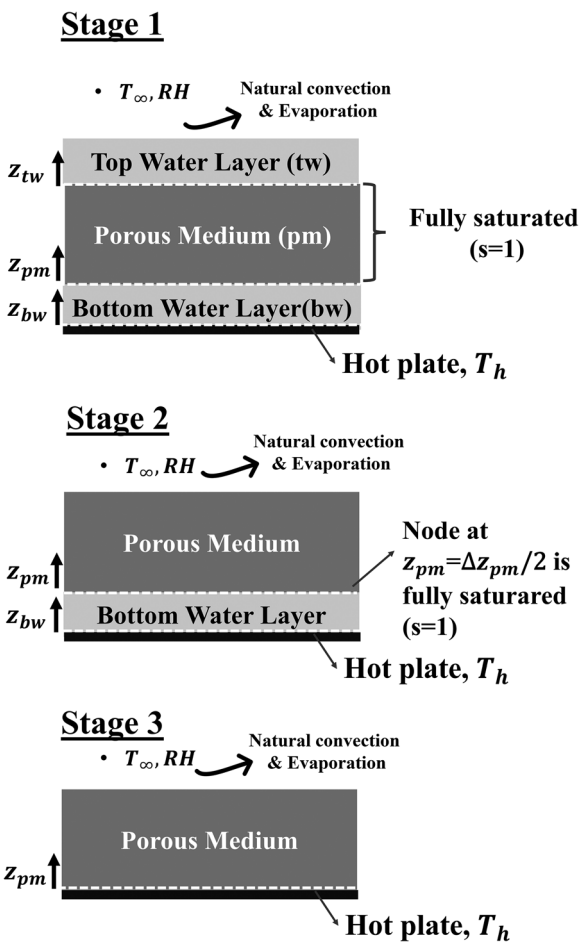

Fig. 2 The three stages during drying of saturated porous media with excess water layers

Governing Equations. Although the current model may be applied to many other porous medium types, this study considers a paper sample as the porous medium. Therefore, a paper-drying model simulating the dryer section of a papermaking machine developed by Asensio and Seyed-Yagoobi [12] is used to develop the current model. This model is aimed at modeling the removal of free water and does not consider the removal of bound water (the trapped moisture inside fibers.) However, the example model [12] is developed for paper with $s \leq 1$ and therefore needs many modifications to account for excess water. It uses the conservation of mass equation (Eq. (6)) and energy equation (Eq. (7)) as the governing equations for the porous medium

$$\frac{\partial M}{\partial t} = -\frac{\partial J_w}{\partial z} - \frac{\partial J_v}{\partial z} \tag{6}$$

$$\left(c_w \rho_w s\varepsilon + c_f \rho_f (1-\varepsilon)\right) \frac{\partial T}{\partial t} = -\frac{\partial q''}{\partial z} - \frac{\partial [J_w H_w + J_v H_v]}{\partial z} \tag{7}$$

where

$$q'' = -k_{\text{eff}} \frac{\partial T}{\partial z} \quad \text{Fourier's Law} \tag{8}$$

$$J_w = \left(\frac{K}{v_w}\right) \frac{\partial P_{\text{ca}}}{\partial z} \quad \text{Darcy's Law} \tag{9}$$

$$J_v = -\left(\frac{D_{ap} M W_v}{1 - y_v}\right) \frac{\partial C_v}{\partial z} \quad \text{Fick's Law} \tag{10}$$

The governing equations used for each drying stage are detailed as follows. During stage 1, since the porous medium is fully saturated, the water and vapor mass fluxes across the thickness direction are zero. Therefore, the mass equation is redundant, and only the energy equation (Eq. (7)) accounts for the porous medium. In the model, the saturation of the porous medium is set as unity, but $\text{DBMC}_{\text{pm},s=1}$ is calculated at every time-step. $\text{DBMC}_{\text{pm},s=1}$ declines due to thermal expansion (i.e., the volume of water in each layer, including the porous medium, increases), which means that the porous medium must lose moisture as it heats up. This loss is reflected as a gain in the top water layer, and it is assumed that this discharge does not enter the bottom water layer.

Both water layers exist in stage 1, and the energy equation has to be solved to obtain the temperature profiles of these layers. Since the water layers do not contain fiber, the effective properties are of water, and porosity and saturation are, theoretically, unity. Also, since there is no solid content in the water layers, liquid water and water vapor mass fluxes become zero. When these modifications are applied to the energy equation in Eq. (7), it becomes Eq. (11). This simple transient conduction equation is used to solve both water layers' temperature profiles in stage 1

$$(c_w \rho_w) \frac{\partial T}{\partial t} = -\frac{\partial q''}{\partial z} \tag{11}$$

Moreover, during stage 1, the water layer thicknesses are tracked. The top water layer thickness changes as a result of three factors: (1) Water evaporation from the surface, (2) Water density variation depending on the temperature profile, and (3) "Additional" excess water is discharged by the porous medium due to thermal expansion. All of these factors are accounted for in

Eq. (12), where $J_{v,o}$ is the vapor flux due to surface evaporation by Eq. (13), and M_d is the discharged water mass added to the top water layer by Eq. (14). Note that the average density of water ($\overline{\rho}_{tw}$ or $\overline{\rho}_{bw}$) is calculated by averaging the water densities across that water layer using the local temperature values. In addition, $\overline{\mathrm{DBMC}}_{\mathrm{next}}$ is calculated by combining the conservation of mass equation in Eq. (6) and the relation between M and DBMC by Eq. (4).

$$\mathrm{th}_{\mathrm{tw}}|_{\mathrm{next}} = \frac{(\overline{\rho}_{\mathrm{tw}}\mathrm{th}_{\mathrm{tw}})_{\mathrm{prev}} - J_{v,o}\Delta t + M_d \mathrm{th}_{\mathrm{pm}}}{\overline{\rho}_{\mathrm{tw}}|_{\mathrm{next}}} \tag{12}$$

$$J_{v,o} = k_m\left(\frac{P_v - P_{v,a}}{P_{\mathrm{atm}}}\right) \tag{13}$$

$$M_d = \frac{\mathrm{BW}\,(\overline{\mathrm{DBMC}}_{\mathrm{prev}} - \overline{\mathrm{DBMC}}_{\mathrm{next}})_{\mathrm{pm},s=1}}{\mathrm{th}_{\mathrm{fin}}} \tag{14}$$

For stage 1, the bottom water layer's thickness ($\mathrm{th}_{\mathrm{bw}}$) is only altered by thermal expansion, which is shown in the following equation:

$$\mathrm{th}_{\mathrm{bw}}|_{\mathrm{next}} = \frac{(\overline{\rho}_{\mathrm{bw}}\mathrm{th}_{\mathrm{bw}})_{\mathrm{prev}}}{\overline{\rho}_{\mathrm{bw}}|_{\mathrm{next}}} \tag{15}$$

During stage 2, since the porous medium is free to evaporate from its top surface, the mass (Eq. 6) and energy (Eq. (7)) equations are solved. The bottom layer's temperature profile is found through the transient conduction equation given in Eq. (14). The $\mathrm{th}_{\mathrm{bw}}$ is updated by Eq. (16), where $J_{w,i}$ is the liquid flux entering the porous medium, which is sourced by the bottom layer. The calculation for $J_{w,i}$ is described in the "Boundary Conditions" section.

$$\mathrm{th}_{\mathrm{bw}}|_{\mathrm{next},2} = \frac{(\overline{\rho}_{\mathrm{bw}}\mathrm{th}_{\mathrm{bw}})_{\mathrm{prev}} - J_{w,i}\Delta t}{\overline{\rho}_{\mathrm{bw}}|_{\mathrm{next}}} \tag{16}$$

In stage 3, only the porous medium layer remains, and the mass (Eq. (6)) and energy (Eq. (7)) conservation equations are solved in the interior nodes. Asensio and Seyed-Yagoobi [12]'s paper shrinkage and porosity model are utilized throughout the drying process. Furthermore, an experimental capillary pressure correlation [30] of linerboard paper is inputted into the model. Also, the mole fraction of vapor (y_v), apparent vapor diffusivity (D_{ap}), and molar vapor concentration (C_v) are calculated using the equations reported in Bell [31] and Asensio and Seyed-Yagoobi [12].

As aforementioned, this study uses the shrinkage model of Asensio and Seyed-Yagoobi [12], where the instantaneous thickness of the porous medium (paper) is a function of span-averaged DBMC, final (bone-dry) thickness and sheet temperature, and is given as follows:

$$\mathrm{th}_{\mathrm{pm}} = \mathrm{th}_{\mathrm{pm,fin}} + \frac{\overline{\mathrm{DBMC}}\cdot \mathrm{BW}}{\overline{\rho_w}} \tag{17}$$

Boundary Conditions. Tables 1–3 summarize the boundary conditions of each layer for stages 1–3, respectively. The initial conditions are presented later in the paper in Table 4. In the numerical solution, interfaces between two layers (e.g., bw–pm, pm–tw) and boundary nodes are half a step size ($\Delta z/2$) away from the interfaces. Interfaces are only surface nodes and do not have a volume whereas boundary nodes have a "volume" of Δz. Therefore, for each physical boundary, there is a boundary node for each layer with a corresponding boundary equation. At the actual interfaces, the flux rate leaving one side is the same as the heat flux rate received at the other side. Furthermore, the saturation of the porous medium is set at unity at both boundaries during stage 1 and its bottom boundary during stage 2. Other than these conditions, the moisture content of the porous medium's boundary nodes is calculated by the mass equation. Moreover, the convective heat transfer is estimated by the natural convection correlations [29] of a horizontal isothermal surface and by inputting the surface temperature of the top surface (of either the top water layer surface or the porous medium, depending on the drying stage.) The heat and mass transfer are connected by applying the Chilton-Colburn analogy. The vapor flux exiting the surface due to evaporation is the $J_{v,o}$ term at the surface node boundary conditions.

During Stage 2, the bottom layer dries, while the moisture of the bottom layer penetrates the porous medium layer. This condition is represented by a liquid mass flux entering the porous medium ($J_{w,\mathrm{i}}$), sourced by the bottom water layer. $J_{w,\mathrm{i}}$ is calculated by back-calculating the liquid mass flux required to maintain the saturation at unity at the bottom boundary node of the porous medium. Therefore, the mass equation at $z_{\mathrm{pm}} = \Delta z_{\mathrm{pw}}/2$ that is given in Eq. (18) is manipulated to attain the liquid flux entering the porous medium, to ensure a full saturation level at this node. This is shown in Eq. (19)

$$\frac{\partial M_{s=1}}{\partial t} = \frac{1}{\Delta z}(-J_w + J_{w,\mathrm{i}}) \tag{18}$$

$$J_{w,\mathrm{i}} = \frac{\Delta z}{\Delta t}\left(M_{\mathrm{prev}} - M_{\mathrm{next}}\right)_{s=1} + J_w \tag{19}$$

Numerical Methodology

The governing equations and boundary conditions given in the "Theoretical Model" section were solved numerically using MATLAB. Finite differencing methods were utilized for spatial (second-order) and temporal (first-order) discretization. Time-dependent terms were discretized based on the fully explicit Euler method. Each layer (tw, bw, and pm) is divided into a certain number of equally distanced nodes (N_{tw}, N_{bw}, and N_{pm}), and where the distance between two nodes within a layer is Δz. At each layer, the first and last nodes are half a step size ($\Delta z/2$) into the layer from the actual boundaries, and these nodes are assumed as the boundary nodes. The time-step size (Δt_1, Δt_2, and Δt_3) of each stage of drying and the node numbers (N_{tw}, N_{bw}, and N_{pm}) for each layer were determined based on time-step and mesh-independent solutions and the stability of the model. The reported results were generated using 10^{-5}s, 10^{-7}s, and 10^{-5}s for Δt_1, $\Delta t_2$and Δt_3, and 6, 6, and 12 for N_{tw}, N_{bw}, and N_{pm}, respectively. Since the model assumes ignorable/minimal Rayleigh–Bénard convection in the excess water layers, the conduction problem in these layers does not require many nodes based on the conducted mesh independence study. In addition, the excess water layers are considered dried when a stopping criterion of $\mathrm{th}_w < 10^{-6}$m was satisfied for each layer.

Validation of the Theoretical Model

Numerical predictions are compared with paper-drying experimental data. Yang et al. [32] conducted paper drying experiments where a moist sheet with excess water is dried on a hot plate. They presented the heat flux rate underneath the moist paper and total moisture content during the drying process. The heat flux rate given in Fig. 3 is used as q'' term in the boundary condition equations tabulated in Table 1, Table 2 and Table 3. After $t = 1100$ s, the paper lifts off from the hot plate due to bulging; hence, the data are shown until the liftoff. In addition, the top boundary condition is prescribed as the Dirichlet-type boundary condition in the model, where temperature is equated to the sample's average top surface temperature measured by an IR camera. A minor adjustment had to be made at the boundary condition above since the immediate humidity level above the sample was unknown. The surface temperature measurement of the sample

Table 1 Boundary conditions of stage 1

Stage 1—boundary conditions	
Interface (hot plate)	
$z_{bw} = 0$	• $T = T_h$
Bottom water layer (bw)	
$z_{bw} = \frac{\Delta z_{bw}}{2}$	• $(c_w \rho_w)\frac{\partial T_{bw}}{\partial t} = \frac{1}{\Delta z_{bw}}\left(q'' + k_w \frac{\partial T_{bw}}{\partial z}\right)$ Where $q'' = \left(k_w \frac{T_h - T_{bw}}{\Delta z_{bw}/2}\right)$ for the example case
$z_{bw} = th_{bw} - \Delta z_{bw}/2$	• $(c_w \rho_w)\frac{\partial T_{bw}}{\partial t} = \frac{1}{\Delta z_{bw}}\left(-k_w \frac{\partial T_{bw}}{\partial z} + k_w \frac{T_{bwpm} - T_{bw}}{\Delta z_{bw}/2}\right)$
Interface (bw–pm)	
$z_{pm} = 0$ OR $z_{bw} = th_{bw}$	$T = T_{bwpm}$ • $k_w \frac{T_{bwpm} - T_{bw}}{\Delta z_{bw}/2} = k_{eff} \frac{T_{pm} - T_{bwpm}}{\Delta z_{pm}/2}$, after solving for T_{bwpm} : $T_{bwpm} = \frac{\frac{k_{eff}}{\Delta z_m} T_{pm} + \frac{k_w}{\Delta z_{bw}} T_{bwpm}}{\left(\frac{k_w}{\Delta z_{bw}} + \frac{k_{eff}}{\Delta z_{pm}}\right)}$
Porous medium (pm)	
$z_{pm} = \Delta z_{pw}/2$	• $(c\rho)_{eff}\frac{\partial T_{pm}}{\partial t} = \frac{1}{\Delta z_{pm}}\left(-k_{eff}\frac{T_{pm} - T_{bwpm}}{\Delta z_{pm}/2} + k_{eff}\frac{\partial T_{pm}}{\partial z}\right)$ • $s = 1$
$z_{pm} = th_{pm} - \frac{\Delta z_{pm}}{2}$	• $(c\rho)_{eff}\frac{\partial T_{pm}}{\partial t} = \frac{1}{\Delta z_{pm}}\left(-k_{eff}\frac{\partial T_{pm}}{\partial z} + k_{eff}\frac{T_{pmtw} - T_{pm}}{\Delta z_{pm}/2}\right)$ • $s = 1$
Interface (pm–tw)	
$z_{tw} = 0$ OR $z_{pm} = th_{pm}$	$T = T_{pmtw}$ $k_{eff}\frac{T_{pmtw} - T_{pm}}{\Delta z_{pm}/2} = k_w \frac{T_{tw} - T_{pmtw}}{\Delta z_{tw}/2}$, after solving for T_{pmtw}: $T_{pmtw} = \frac{\frac{k_{eff}}{\Delta z_{pm}} T_{pm} + \frac{k_w}{\Delta z_{tw}} T_{tw}}{\left(\frac{k_w}{\Delta z_{tw}} + \frac{k_{eff}}{\Delta z_{pm}}\right)}$
Top water layer (tw)	
$z_{tw} = \Delta z_{tw}/2$	• $(c_w \rho_w)\frac{\partial T_{tw}}{\partial t} = \frac{1}{\Delta z_{tw}}\left(-k_{eff}\frac{T_{pm} - T_{bwpm}}{\Delta z_{tw}/2} + k_w \frac{\partial T_{tw}}{\partial z}\right)$
$z_{tw} = th_{tw} - \Delta z_{tw}/2$	• $(c_w \rho_w)\frac{\partial T_{tw}}{\partial t} = \frac{1}{\Delta z_{tw}}\left(-k_w \frac{\partial T_{tw}}{\partial z} - J_{v,o}\lambda - h(T_{tw} - T_\infty)\right)$

measured by the IR camera was reduced. Figure 4 shows the total moisture content where numerical predictions aligned well with the experimental data with root-mean-square error (RMSE) = 0.16.

Results and Discussion

The results are given for the "example case" which has slightly different boundary conditions than the "validation case." The example case does not have a prescribed temperature at the top surface and is solved by the energy rate equation, and the bottom surface heat flux is calculated by $q'' = k_w \frac{T_h - T_{bw}}{\Delta z_{bw}/2}$ for Stages 1–2 and $q'' = k_{eff} \frac{T_h - T_{pm}}{\Delta z_{pm}/2}$ for Stage 3.

The parameters of the model are tabulated in Table 4. Due to excess water, the initial total DBMC is much higher than the initial DBMC of the fully saturated porous medium. In addition, the hot-plate's temperature is fixed at a constant temperature (98 °C), below the boiling temperature of water at atmospheric pressure. Furthermore, the initial thickness of excess water layers is calculated by dividing the total excess water thickness by Eq. (2) whereas the initial thickness of the porous medium is calculated by Eq. (17) when the necessary initial values are inserted.

Table 2 Boundary conditions of stage 2

Stage 2—boundary conditions	
Interface (hot plate)	
$z_{bw} = 0$	• $T = T_h$
Bottom water layer (bw)	
$z_{bw} = \Delta z_{bw}/2$	• $(c_w\rho_w)\dfrac{\partial T_{bw}}{\partial t} = \dfrac{1}{\Delta z_{bw}}\left(q'' + k_w\dfrac{\partial T_{bw}}{\partial z}\right)$
	Where $q'' = \left(k_w\dfrac{T_h - T_{bw}}{\Delta z_{bw}/2}\right)$ for the example case
$z_{bw} = th_{bw} - \Delta z_{bw}/2$	• $(c_w\rho_w)\dfrac{\partial T_{bw}}{\partial t} = \dfrac{1}{\Delta z_{bw}}\left(-k_w\dfrac{\partial T_{bw}}{\partial z} + k_w\dfrac{T_{bwpm} - T_{bw}}{\Delta z_{bw}/2} - J_{w,i}H_w\right)$
Interface (bw–pm)	
$z_{pm} = 0$ OR $z_{bw} = th_{bw}$	$T = T_{bwpm}\, k_w\dfrac{T_{bwpm} - T_{bw}}{\Delta z_{bw}/2} = k_{eff}\dfrac{T_{pm} - T_{bwpm}}{\Delta z_{pm}/2}$, after solving for T_{bwpm}: $T_{bwpm} = \dfrac{\frac{k_{eff}}{\Delta z_{pm}}T_{pm} + \frac{k_w}{\Delta z_{bw}}T_{bwpm}}{\left(\frac{k_w}{\Delta z_{bw}} + \frac{k_{eff}}{\Delta z_{pm}}\right)}$
Porous medium (pm)	
$z_{pm} = \Delta z_{pw}/2$	• $(c\rho)_{eff}\dfrac{\partial T_{pm}}{\partial t} = \dfrac{1}{\Delta z_{pm}}\left(-k_{eff}\dfrac{T_{pm} - T_{bwpm}}{\Delta z_{pm}/2} + J_{w,i}H_w + k_{eff}\dfrac{\partial T_{pm}}{\partial z}\right)$
	• $s = 1$
$z_{pm} = th_{pm} - \Delta z_{pm}/2$	• $(c\rho)_{eff}\dfrac{\partial T_{pm}}{\partial t} = \dfrac{1}{\Delta z_{pm}}\left(-k_{eff}\dfrac{\partial T_{pm}}{\partial z} + J_vH_v + J_wH_w - J_{v,o}H_v - h(T_{pm} - T_\infty)\right)$
	• $\dfrac{\partial M}{\partial t} = \dfrac{1}{\Delta z}(J_w + J_{v,i} - J_{v,o})$

Table 3 Boundary conditions of stage 3

Stage 3—boundary conditions	
Interface (hot plate)	
$z_{pm} = 0$	• $T = T_h$
Porous medium (pm)	
$z_{pm} = \Delta z_{pw}/2$	• $(c\rho)_{eff}\dfrac{\partial T_{pm}}{\partial t} = \dfrac{1}{\Delta z_{pm}}\left(q'' + k_{eff}\dfrac{\partial T_{pm}}{\partial z} - J_wH_w - J_vH_v\right)$
	Where $q'' = \left(k_{eff}\dfrac{T_h - T_{pm}}{\Delta z_{pm}/2}\right)$ for the example case
	• $\dfrac{\partial M}{\partial t} = \dfrac{1}{\Delta z}(-J_w - J_v)$
$z_{pm} = th_{pm} - \Delta z_{pm}/2$	• $(c\rho)_{eff}\dfrac{\partial T_{pm}}{\partial t} = \dfrac{1}{\Delta z}\left(-k_{eff}\dfrac{\partial T_{pm}}{\partial z} + J_vH_v + J_wH_w - J_{v,o}H_v - h(T_{pm} - T_\infty)\right)$
	• $\dfrac{\partial M}{\partial t} = \dfrac{1}{\Delta z}(J_w + J_{v,i} - J_{v,o})$

Figure 5 shows the top and bottom water layers' thicknesses with respect to drying time. During Stage 1, the top water layer dries while th_{bw} stays about the same. During stage 2, bottom water layer dries. At $t = 0$, both layers have the same thickness. At the very early stages of drying, both layers' thicknesses increase slightly due to the thermal expansion caused by the elevated temperatures. The effect of thermal expansion is accounted for by the first term on the right-hand side in Eqs. (12) and (15). In addition, the top water layer thickness rises slightly more, due to the water that exits the porous medium when heated. When the temperature of a fully saturated porous medium rises, additional excess water needs to exit the pores, due to thermal expansion or changes in water density. In this model, this additional excess water caused by thermal expansion is modeled in a way that it is only discharged to the top layer. Since the amount of additional excess water is relatively insignificant, this assumption should be acceptable.

The temperature of each layer (T_{bw}, T_{pm}, and T_{tw}) was averaged and plotted, as shown in Fig. 6. The heat penetrates from bottom to top; therefore, as expected, top and bottom water layers

Table 4 Parameters of the numerical study

Parameter	Value
Hot plate surface temperature, T_h	98 °C
Air temperature, T_h	19 °C
Initial Temperature of all layers	18 °C
Relative humidity of air, RH	50%
Initial total DMBC	6.80
Initial porosity of paper	0.86
Bone-dry porosity of paper	0.73
Initial DBMC of the porous media, $DBMC_{pm,init}$	2.04
Initial saturation of the porous media, s_{init}	1.00
Basis weight of the porous media, BW	126 g/m^2
Permeability of porous media, K	10^{-14} m^2
Thermal conductivity of fiber	0.1 W/(m K)
Density of fiber	1500 kg/m^3
Specific heat of fiber	1400 J/(kg K)
Bone-dried thickness of porous media, $th_{pm,fin}$	0.30 mm
Calculated initial thickness of porous media, $th_{pm,init}$	0.56 mm
Calculated initial thickness of top water layer, $th_{tw,init}$	0.30 mm
Calculated initial thickness of bottom water layer, $th_{bw,init}$	0.30 mm

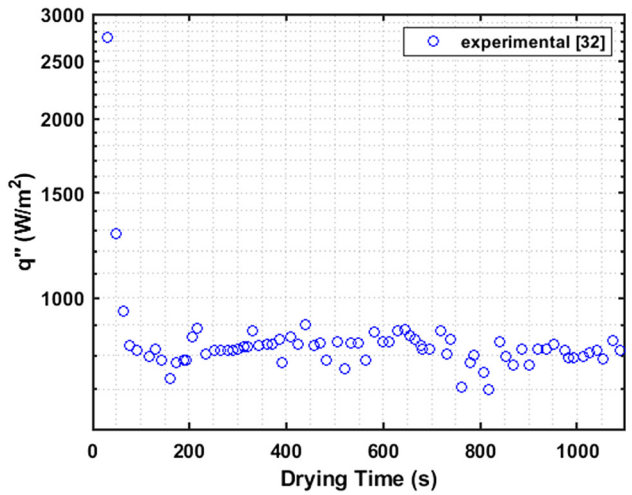

Fig. 3 Experimental surface heat flux measurement of heated plate paper drying obtained from Yang et al. [32]

temperature have the lowest and highest temperatures at a given time, respectively. The decreases in average temperatures are due to the cooling effect of evaporation.

Figure 7 shows the vapor flux at the top boundary due to surface evaporation ($J_{v,o}$) and liquid flux entering the porous media from the bw-pm interface ($J_{w,i}$). As expected, $J_{v,o}$ follows the trends of temperature curves. $J_{w,i}$ is only nonzero during Stage 2 while bw feeds the pm from the bottom. During stage 2, $J_{w,i}$ and $J_{v,o}$ are about the same indicating that pm's moisture content does not decrease while bw dries. This can be further explained with the saturation curve of pm given in Fig. 8. During Stage 1, pm is fully-saturated and $s = 1$. During stage 2, s is very close to 1 and maintains at the same level since moisture entering from pm's bottom is about the same as leaving from its top surface due to evaporation. In stage 3, pm saturation decreases significantly when both water layers are dried up.

Figure 9 displays the heat flux rate at the bottom surface (q'' term in Boundary Condition Tables). The example case's sample dries much faster than that of the validation case because in the validation case q'' is around 850 W/m^2, which is much less than q'' of example case shown in Fig. 9. As expected, q'' is affected by the temperature of the node nearest to the hot plate. Therefore, the q'' curves inversely follow the trends of the temperature curves.

Dry basis moisture content can be calculated not only considering the mass of the water in pm but also factoring in the excess water layers by $DBMC_{total}$. Note that the denominator of

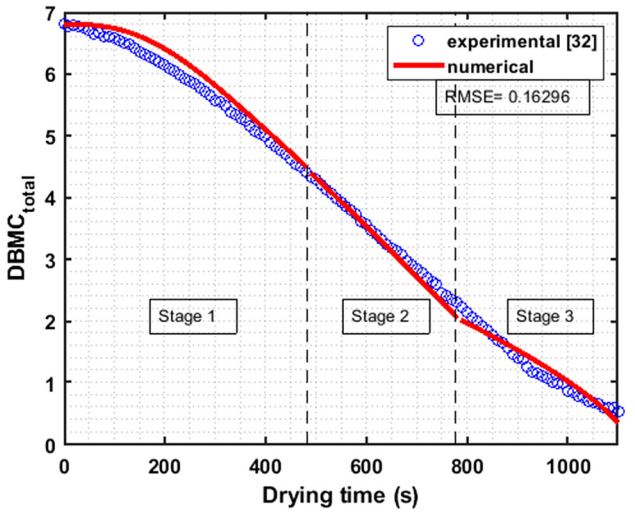

Fig. 4 Validation case—total DBMC of the numerical prediction by the current model versus the experimental measurements obtained from Yang et al. [32]

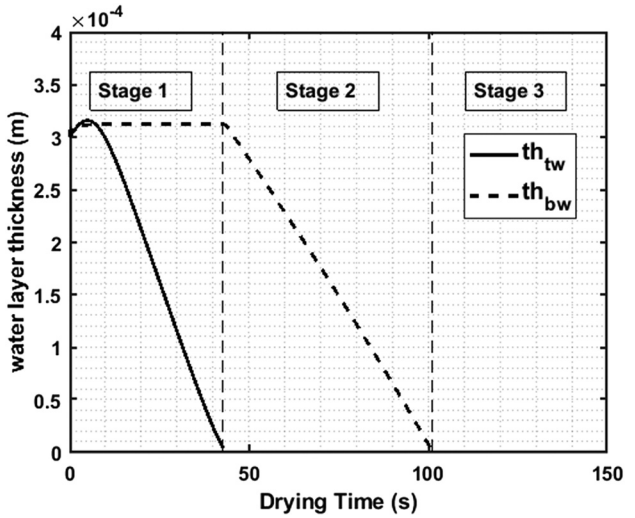

Fig. 5 Example case—the thicknesses of top and bottom water layers versus drying time

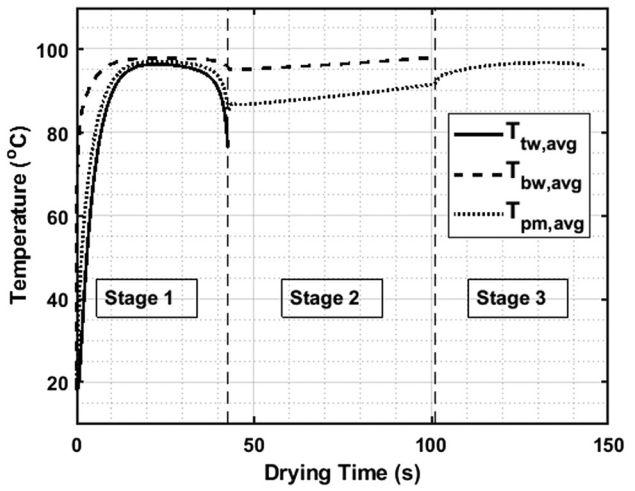

Fig. 6 Example case—average temperature of each layer versus drying time

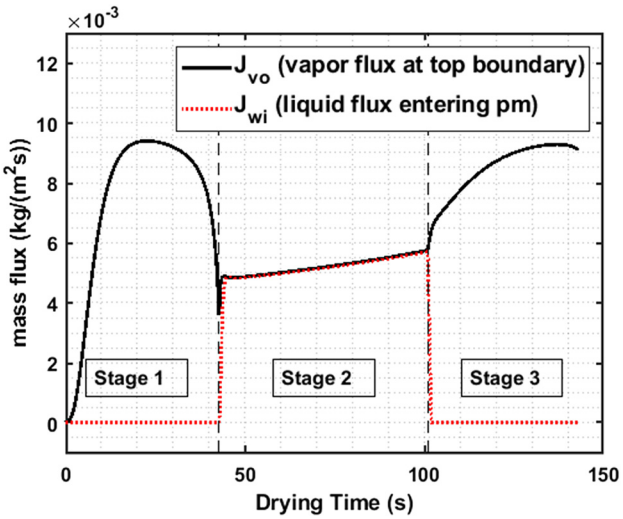

Fig. 7 Example case—vapor flux at the top boundary due to evaporation and liquid flux entering the porous media from its bottom boundary versus drying time

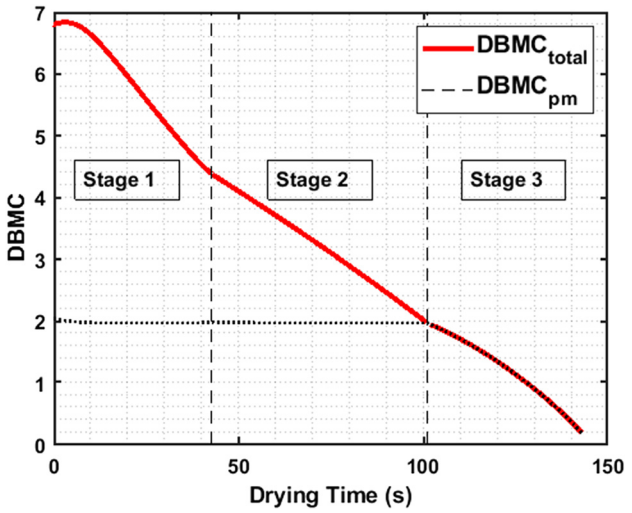

Fig. 10 Example case—total DBMC and DBMC of the porous medium versus drying time

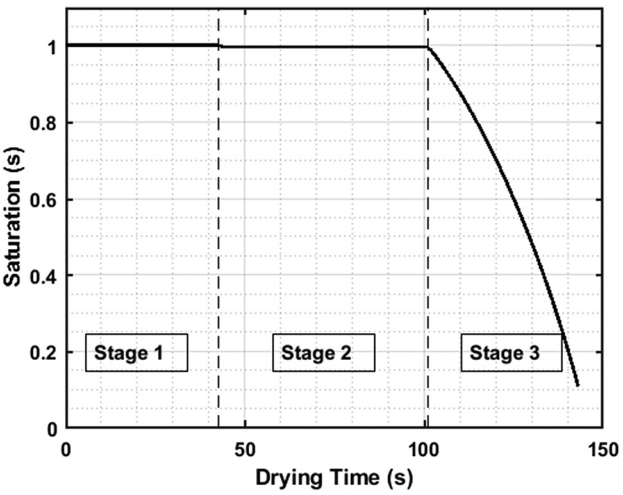

Fig. 8 Example case—saturation of the porous medium versus drying time

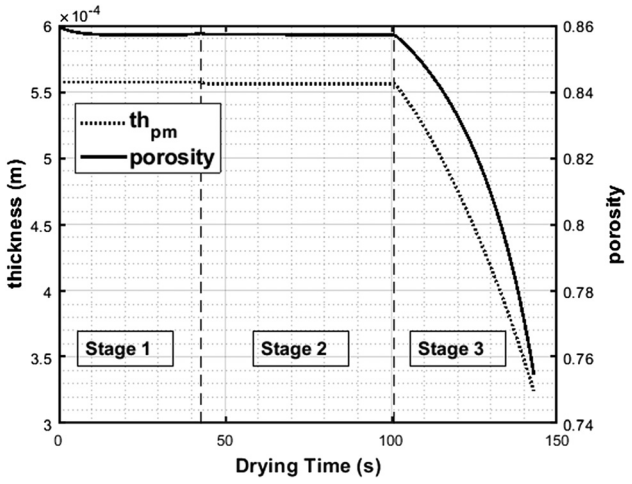

Fig. 11 Example case—thickness and porosity variation of the porous medium during drying

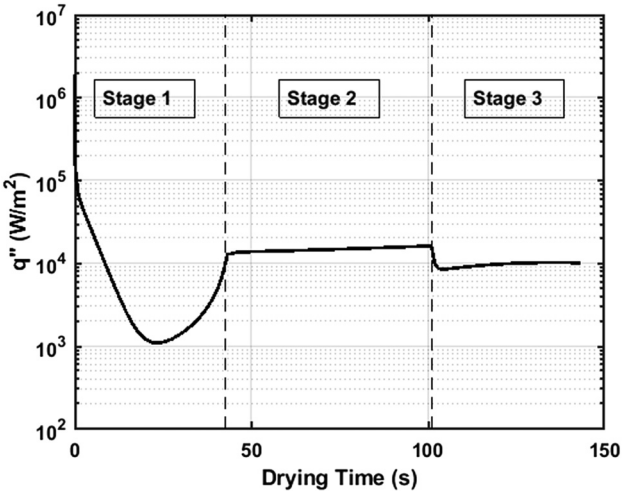

Fig. 9 Example case—surface heat flux rate

$DBMC_{total}$ would be the mass of fiber inside the porous medium, and there would be no contribution from the excess water layers since they do not contain fiber. Both $DBMC_{total}$ and $DBMC_{pm}$ are shown in Fig. 10. $DBMC_{total}$ is much higher than $DBMC_{pm}$ due to the factored-in excess water during stages 1 and 2. However, $DBMC_{total}$ and $DBMC_{pm}$ are the same during stage 3 because, at this stage, the excess water layers have already dried after Stage 2.

The porosity and shrinkage model of Asensio and Seyed-Yagoobi [12] for paper drying was applied. The porosity and paper sheet (pm) thickness results are given in Fig. 11. Since porosity and thickness are a function of moisture content, both curves contain similar behavior to the $DBMC_{pm}$ curves shown in Fig. 10. Compared to the other stages, thickness and porosity decrease the most during stage 3, while the porous medium dries significantly. Both parameters approach their nonzero final value as the porous medium dries.

Conclusions

This paper dealt with the drying of a fully saturated porous medium in the presence of excess water. Specifically, a theoretical model was developed to provide a fundamental understanding of heat and mass transfer in an initially fully saturated moist medium where the excess water was equally divided between its two outer

surfaces. The porous medium considered in this study was a paper sheet, heated from one side, while the evaporation took place from the opposite side. The theoretical model predictions were successfully validated against the corresponding experimental data. The drying process consisted of the following stages.

- Stage 1: The water layer, not in contact with the heated surface, dried completely while the porous medium remained fully saturated.
- Stage 2: Upon the completion of evaporation of the excess water layer exposed to the air, the evaporation started to take place directly from the moist porous medium surface in contact with the air while the water from the opposite excess water layer was fed into the porous medium.
- Stage 3: The excess water layer in contact with the heated plate got depleted, and the porous medium started to drop in its saturation level due to the continued evaporation from its exposed surface to the air. The porous medium eventually lost its moisture while it was heated directly from one side, and the evaporation continued from the opposite side.

This theoretical model can be easily extended to include other means of dehydrating a fully saturated porous medium with excess water, such as microwave, infrared, or ultrasound (in direct-contact or airborne) mechanisms.

Acknowledgment

This study was financially supported by the U.S. Department of Energy, Office of Advanced Manufacturing under Award Number DE-EE0009125, Massachusetts Clean Energy Center (MassCEC) and Center for Advanced Research in Drying (CARD), a U.S. National Science Foundation Industry University Cooperative Research Center. CARD is located at Worcester Polytechnic Institute and the University of Illinois at Urbana-Champaign (cosite).

Funding Data

- U.S. Department of Energy, Office of Advanced Manufacturing (Award No. DE-EE0009125; Funder ID: 10.13039/100000015).

Nomenclature

BW = basis weight; mass of dry sheet/ sheet area (kg/m^2)
bw = bottom excess water layer
bwpm = bw–pm interface
C = molar concentration (kg mol/m^3)
c = specific heat (J/(kg K))
$(c\rho)_{\text{eff}}$ = effective $c\rho$ for porous medium (J/(m^{3}K)); $c_w\rho_w s\varepsilon + c_f\rho_f(1-\varepsilon)$
DBMC = dry basis moisture content; weight of water/weight of dry fibers
$\text{DBMC}_{\text{total}}$ = DBMC considering all the layers (i.e., factoring-in the excess wayer layers)
D = diffusivity (m^2/s)
H = enthalpy (J/kg)
J = mass flux (kg/(m^{2}s)]
k = thermal conductivity (W/(m K))
K = permeability (m^2)
k_{eff} = effective thermal conductivity of the porous medium (W/(m K)); $(1-\varepsilon)k_f + s\varepsilon k_w + (1-s)\varepsilon k_a$
k_m = mass transfer coefficient (kg/(m^2 s))
M = mass of liquid water in paper sheet (kg/m^3)
MW = molecular weight (kg/kmol)
P = pressure (Pa)
pm = porous medium
pmtw = pm–tw interface
RH = relative humidity (%)
q'' = heat flux (W/(m^2))
s = saturation; volume of liquid/ volume of voids
T = temperature (K)
t = time (s)
th = thickness (m)
tw = top excess water layer
y = mole fraction
z = axis across the thickness of layers
ε = porosity; volume of voids/ total volume
ρ = density (kg/m^3)
Δz = step size or distance between two nodes (m)
λ = change in enthalpy of vaporization (J/kg)

Subscripts

a = air
ap = apparent
atm = atmosphere
bw = bottom excess water layer
ca = capillary
d = discharge
eff = effective
f = fiber
fin = final (bone-dry)
h = hot surface
init = initial
next = next time step after the previous time step
pm = porous medium layer
prev = previous time step (i.e. prior to the next time step)
$s = 1$ = when fully saturated
tw = top excess water layer
v = water vapor
v, o = water vapor exiting the porous medium or top water layer
w = liquid water
w, e = excess water (layer)
w, i = liquid water entering the porous medium
1–3 = stage 1, 2, or 3 of drying
∞ = ambient or infinity

Accent.

$\bar{\cdot}$ = averaged over the nodes in that layer in the thickness direction

References

[1] McMillan, C., Boardman, R., McKella, M., Sabharwall, P., Ruth, M., and Bragg-Sitton, S., 2016, "Generation and Use of Thermal Energy in the U.S. Industrial Sector and Opportunities to Reduce Its Carbon Emissions," Joint Institute of Strategic Energy Analysis, Report No. NREL/TP-6A50-66763.
[2] Stenström, S., 2020, "Drying of Paper: A Review 2000–2018," Drying Technol., **38**(7), pp. 825–845.
[3] Mujumdar, A. S., 1987, *Handbook of Industrial Drying*, Dekker, New York.
[4] Zhang, Y., and Abatzoglou, N., Design, 2020, "Fundamentals, Applications and Potentials of Ultrasound-Assisted Drying," Chem. Eng. Res. Des., **154**, pp. 21–46.
[5] Asar, M. E., Noori, Z., and Yagoobi, J., 2022, "Numerical Investigation of the Effect of Ultrasound on Paper Drying," TAPPI J., **21**(3), pp. 127–140.
[6] Martynenko, A., and Kudra, T., 2016, "Electrically-Induced Transport Phenomena in EHD Drying–a Review," J. Trends Food Sci. Technol., **54**, pp. 63–73.
[7] Patel, V. K., Kyle Reed, F., Kisner, R., Peng, C., Moghaddam, S., and Mehdizadeh Momen, A., 2019, "Novel Experimental Study of Fabric Drying Using Direct-Contact Ultrasonic Vibration," ASME J. Therm. Sci. Eng. Appl., **11**(2), p. 021008.
[8] Asar, M. E., Noori, Z., and Yagoobi, J., 2021, "Preliminary Numerical Investigation of the Effect of Ultrasound on Paper Drying," 21TAPPICon Virtual.
[9] Yang, M., and Yagoobi, J., 2021, "Enhancement of Drying Rate of Moist Porous Media With Dielectrophoresis Mechanism," Drying Technol., epub, pp. 1–12.
[10] Nissan, A., and Hansen, D., 1960, "Heat and Mass Transfer Transients in Cylinder Drying: Part I. Unfelted Cylinders," AIChE J., **6**(4), pp. 606–611.
[11] Seyed-Yagoobi, J., Bell, D., and Asensio, M., 1992, "Heat and Mass Transfer in a Paper Sheet During Drying," ASME J. Heat Transfer-Trans. ASME, **114**(2), pp. 538–541.
[12] Asensio, M. C., and Seyed-Yagoobi, J., 1993, "Simulation of Paper-Drying Systems With Incorporation of an Experimental Drum/Paper Thermal Contact Conductance Relationship," ASME J. Energy Resour. Technol., **115**(4), pp. 291–300.
[13] Seyed-Yagoobi, J., Sikirica, S. J., and Counts, K. M., 2001, "Heating/Drying of Paper Sheet With Gas-Fired Infrared Emitters—Pilot Machine Trials," Drying Technol., **19**(3–4), pp. 639–651.

[14] Hoshi, Y., Kuno, H., Takeshita, K., Hashimoto, R., Yanagi, K. I., and Yoshida, S., 2001, "Prediction of Temperature and Moisture Content Profiles of Paper in a Drying Process," ASME J. Heat Transfer-Trans. ASME, **30**(2), pp. 77–94.
[15] Lu, T., and Shen, S., 2007, "Numerical and Experimental Investigation of Paper Drying: Heat and Mass Transfer With Phase Change in Porous Media," Appl. Therm. Eng., **27**(8–9), pp. 1248–1258.
[16] Sadeghi, M., and Douglas, W. M., 2004, "From Tissue to Linerboard: Validation of a Microscale Simulator for Single Technique and Hybrid Dryers," Proceedings of 14th International Drying Symposium, Saõ Paulo, Brazil, pp. 444–451.
[17] Sadeghi, M., 2003, "Modeling and Simulation of Transport Phenomena in Paper Drying," Doctor of Philosophy Thesis, McGill University, Montreal, QC, Canada.
[18] Anjomshoaa, A., and Salmanzadeh, M., 2022, "A Novel Thermodynamic and Heat and Mass Transfer Model for the Multicylinder Dryer Section of a Paper Machine," Drying Technol., **40**(7), pp. 1307–1328.
[19] Kong, L., Tao, Z., Liu, H., and Zhang, D., 2016, "Effect of Operating Parameters on the Drying Performance of Multicylinder Paper Machine Dryer Section," Drying Technol., **34**(13), pp. 1641–1650.
[20] Zvolinschi, A., Johannessen, E., and Kjelstrup, S., 2006, "The Second-Law Optimal Operation of a Paper Drying Machine," J. Chem. Eng. Sci., **61**(11), pp. 3653–3662.
[21] Martín, E., Viéitez, I., and Varas, F., 2021, "A Predictive Model for the Industrial Air-Impingement Drying of Resin Impregnated Paper," Appl. Therm. Eng., **199**, p. 117602.
[22] Whitaker, S., 1977, "Simultaneous Heat, Mass, and Momentum Transfer in Porous Media: A Theory of Drying," *Advances in Heat Transfer*, Elsevier. pp. 119–203.
[23] Coumans, W., 1994, "Transport Parameters and Shrinkage in Paper Drying," Proceedings of 9th International Drying Symposium (IDS '94), V. Rudolph, and R. B. Keey, eds., Elsevier, Amsterdam, The Netherlands, pp. 1205–1212.
[24] Harrmann, M., and Schulz, S., 1990, "Convective Drying of Paper Calculated With a New Model of the Paper Structure," Drying Technol., **8**(4), pp. 667–703.
[25] Asensio, M., and Seyed-Yagoobi, J., 1992, "Theoretical Drying Study of Single-Tier Versus Conventional Two-Tiered Dryer Configurations," TAPPI J., **75**(10), pp. 203–211.
[26] Yan, Y., Jiangli, P., Jixian, D., and Jian, S., 2022, "Study on Paper Drying Rate Based on Lattice Boltzmann Method," J. Korea TAPPI, **54**(1), pp. 10–17.
[27] Vu, H. T., and Tsotsas, E., 2018, "Mass and Heat Transport Models for Analysis of the Drying Process in Porous Media: A Review and Numerical Implementation," Int. J. Chem. Eng., **2018**, pp. 1–13.
[28] Carbonell, M., Virto, L., and Gamez-Montero, P. J., 2018, "Dryout and Replenishment of Bottom-Heated Saturated Porous Media With an Overlying Plain Water Layer," Appl. Sci., **8**(12), p. 2607.
[29] Incropera, F. P., Lavine, A. S., Bergman, T. L., and DeWitt, D. P., 2013, *Principles of Heat and Mass Transfer*, Wiley, Hoboken, NJ.
[30] Asensio, M. C., 2000, "Transport Phenomena During Drying of Deformable, Hygroscopic Porous Media: Fundamentals and Applications," Ph.D. dissertation, Texas A & M University, College Station, TX.
[31] Bell, D. O., 1990, "Theoretical and Numerical Analysis of Heat and Mass Transfer in Paper Sheet During Drying," M.S. thesis, Texas A&M University, College Station, TX.
[32] Yang, M., Asar, M. E., and Yagoobi, J., 2021, "Experimental Study of Heat Transfer Characteristics of Drying Process With Dielectrophoresis Mechanism," ASME Paper No. IMECE2021-69545.